npj | quantum information

Article

Published in partnership with The University of New South Wales

https://doi.org/10.1038/s41534-026-01220-3

Robust photon blockade with hybrid molecular optomechanics

Check for updates

Jian Tang[1], Baijun Li[2], Bin Yin[1], Tian-Xiang Lu[3], Ran Huang[4] ✉, Franco Nori[4,5] & Hui Jing[1,6] ✉

Molecular cavity optomechanical systems, featuring ultrahigh vibrational frequencies and strong light-matter interactions, hold significant promise for advancing applications in quantum science and technology. Specifically, by introducing metallic nanoparticles into microcavities, hybrid molecular cavity optomechanical systems can further enhance optical quality factors and system tunabilities, which enable scalable and controllable quantum platforms. In this study, we propose how to realize robust photon blockade, i.e., strong photon antibunching with arbitrary detuning conditions, by combining degenerate optical parametric amplification with a hybrid molecular cavity optomechanical system. More interesting, we find near-perfect optomechanical photon blockade at room temperature, which is robust against temperature and optical dissipation. In addition, our approach can release the strict condition of high temporal resolution by combining features of conventional and unconventional photon blockade. Our approach offers a feasible route to study intriguing quantum effects in hybrid molecular cavity optomechanical systems, and holds promise for applications in nonclassical state engineering, quantum sensing, and photonic precision measurements.

Cavity optomechanical systems[1,2], characterized by the interaction between optical fields and mechanical vibrations, offer a versatile platform for both fundamental research in physics and potential applications in high-precision sensing[3–9]. Specifically, molecular vibrations, serving as nanoscale mechanical oscillators, exhibit exceptionally high resonant frequencies and strong optomechanical interactions with optical fields[10–12]. These features enable molecular cavity optomechanical systems to be remarkably resistant to temperature fluctuations and variations in system parameters. Therefore, molecular cavity optomechanical systems are ideal for applications such as heat transfer[13], optomechanically induced transparency[14], frequency up-conversion[15–17], metrology[18–20], surface-enhanced Raman scattering[21], phonon parametric amplification[22] and molecular-protein analysis[23], as well as quantum heat engine[24], and entanglement[25].

Recent technological advances have enabled the integration of nanoparticles into high-quality microcavity platforms[26]. Hybrid molecular cavity optomechanical systems[27–30] have been proposed and studied using metallic nanoparticles combined with Fabry-Pérot resonators[27], whispering-gallery-mode resonators[28,29], or photonic crystals[30]. These hybrid platforms not only retain the high resonant frequencies and strong optomechanical interactions, but also exhibit higher optical quality factors[27,29–31], exhibiting broad potential for various applications, such as microfilters and miniature spectrometers[32]. More importantly, the platforms enhance the scalability of molecular optomechanical systems, enabling flexible control via coupled cavity configurations.

Optical parametric amplification is a second-order nonlinear process, in which an optical signal is amplified by a pump via the generation of an idler field[33], and can be used to realize sources of biphotons[34–36], squeezed light[37–40], and highly nonclassical states of light[41,42]. Despite the inherently weak second-order nonlinearity, the large parametric gain can be achieved through strong pumping. Optical parametric amplification has been used to realize nonreciprocal optical transistor[43], phonon lasing[44], as well as entanglement between two atoms[45], long-lived or entangled cat states[46,47], tripartite quantum entanglement[48], quantum sensing[49,50], and photon blockade[51–53]. In the weak pump regime, the nonlinear process can be seen as a different excitation path[52]. This nonlinear process gives rise to destructive quantum interference between transition pathways, which is the fundamental mechanism of unconventional photon blockade[54–61]. Such a nonlinear process-induced photon blockade has been predicted in various platforms, including spinning cavity[62], coupled cavities[63], and cavity optomechanics[64,65].

In this work, we propose how to realize a robust photon blockade scheme by introducing a degenerate optical parametric amplifier within a

[1]Key Laboratory of Low-Dimensional Quantum Structures and Quantum Control of the Ministry of Education, Hunan Normal University, Changsha, China. [2]Research Center for Quantum Physics, Huzhou University, Huzhou, China. [3]College of Physics and Electronic Information, Gannan Normal University, Ganzhou, Jiangxi, China. [4]Quantum Information Physics Theory Research Team, Quantum Computing Center, RIKEN, Wako-shi, Saitama, Japan. [5]Physics Department, The University of Michigan, Ann Arbor, MI, USA. [6]College of Science, NUDT, Changsha, People's Republic of China. ✉e-mail: ran.huang@riken.jp; jinghui73@foxmail.com

hybrid molecular cavity optomechanical system. Specifically, by tuning the intensity and phase of the parametric gain, we can achieve strong photon antibunching under arbitrary detuning conditions. More interesting, we find near-perfect optomechanical photon blockade ($g^{(2)}_{\min}(0) \sim 0.00001$) at room temperature, which is robust against temperature and optical dissipation. Furthermore, we find that the oscillations in $g^{(2)}(\tau)$ can be eliminated, thus releasing the strict condition of high temporal resolution in experimental detection. Our approach offers a feasible route to achieve robust photon blockade using existing hybrid molecular cavity optomechanical platforms and holds promise for applications in nonclassical state engineering, quantum sensing, and photonic precision measurements.

Results

Model

We consider the following hybrid molecular cavity optomechanical system. A nanoparticle-on-mirror (NPoM) structure consists of a metallic nanoparticle deposited on a mirror coated with a metallic film, which forms a plasmonic nanocavity that resonates at frequency ω_c, as shown in the inset in Fig. 1a[66–68]. A molecule is positioned in the nanoscale gap between the nanoparticle and the mirror, and is considered as a harmonic oscillator with a resonance frequency ω_b and a damping rate γ. This molecule couples to the plasmonic field via optomechanical interaction. By introducing an additional mirror, a Fabry-Pérot cavity is formed with resonance frequency ω_c, which contains a degenerate optical parametric amplifier. These components together form the hybrid molecular optomechanical system, as shown in Fig. 1a.

To achieve photon antibunching, we coherently drive the plasmonic nanocavity with a weak external field at frequency ω_L. Through the coupling between the two cavities (with strength J), this excitation populates the Fabry-Pérot cavity mode, which then interacts with the optical parametric amplifier driven by an external laser at frequency ω_p. The Hamiltonian for this three-mode system can be expressed as (assuming $\hbar = 1$):

$$\begin{aligned}
\hat{H}_1 &= \omega_a \hat{a}^\dagger \hat{a} + \omega_c \hat{c}^\dagger \hat{c} + \omega_b \hat{b}^\dagger \hat{b} + \hat{H}_j + \hat{H}_d, \\
\hat{H}_j &= J(\hat{a}^\dagger \hat{c} + \hat{c}^\dagger \hat{a}) + g\hat{c}^\dagger \hat{c}(\hat{b}^\dagger + \hat{b}), \\
\hat{H}_d &= \xi(\hat{c} e^{i\omega_L t} + H.c.) + \Omega(\hat{a}^2 e^{i\theta} e^{i\omega_p t} + H.c.),
\end{aligned} \tag{1}$$

where $\hat{a}(\hat{a}^\dagger)$, $\hat{c}(\hat{c}^\dagger)$, and $\hat{b}(\hat{b}^\dagger)$ represent the annihilation (creation) operators for the Fabry-Pérot cavity mode, the plasmonic nanocavity mode, and the molecular vibrational mode (phonons), respectively. Here, $g\hat{c}^\dagger \hat{c}(\hat{b}^\dagger + \hat{b})$ describes the optomechanical coupling interaction between the plasmonic nanocavity mode and the molecular vibrations. The coupling strength is given by $g = -\omega_c R_b \sqrt{\hbar/2m\omega_b}/(\varepsilon_0 V_c)$[11,12], where R_b is the Raman polarizability, V_c is the effective volume of the plasmonic nanocavity mode, and ε_0 is the vacuum permittivity. In this work, we take as $R_b = 3\times 10^{-10}\ \varepsilon_0^2 \ddot{A}^4 \mathrm{amu}^{-1}$, and $V_c = 2.5\mu\mathrm{m}^{-7}$[11,12], which yield $g/2\pi =$

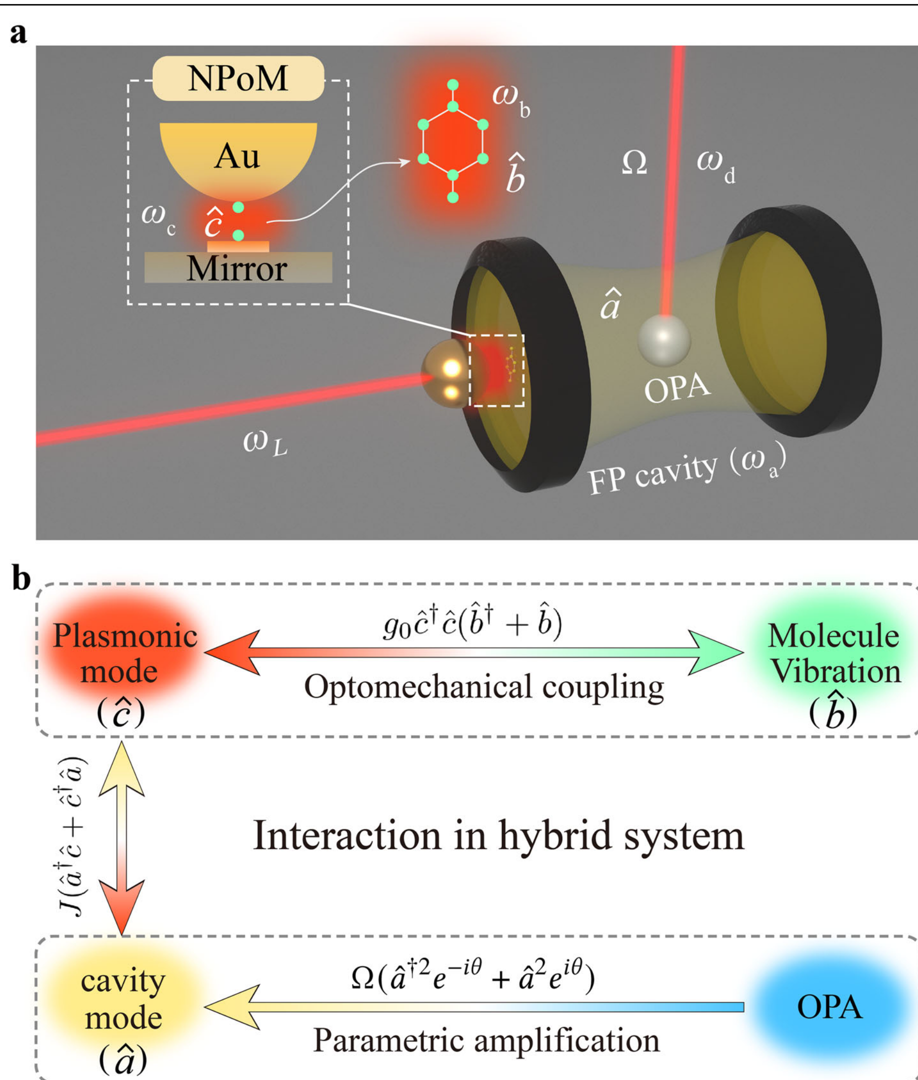

Fig. 1 | Parametric amplification assistant hybrid molecule cavity optomechanical system. **a** Schematic of the hybrid molecule cavity optomechanical system. A plasmonic nanocavity, formed by metallic nanoparticles and molecules deposited on a Fabry-Pérot (FP) cavity, is driven by an external laser of frequency ω_L. A degenerate optical parametric amplifier (OPA) inside the Fabry-Pérot cavity is driven by a laser of amplitude Ω and frequency ω_d. The inset shows the nanoparticle-on-mirror (NPoM) structure of the plasmonic nanocavity, where molecules are situated in the nanogap between the nanoparticle and a mirror coated with a thin metallic film. **b** Schematic diagram of the equivalent mode-coupling model. The plasmonic nanocavity mode is coupled to the molecular vibrational (acoustic) mode via radiation pressure. This mode is also coupled to the FP cavity mode (incorporating the parametric process) through evanescent field interactions.

30GHz. The optomechanical coupling coefficient g is estimated on the order between from $2\pi \times 10$GHz to $2\pi \times 100$GHz, and from $\omega_b/2\pi \sim 6$THz to 48THz[10–12]. The driving amplitude ξ is expressed as $\xi = \left[\gamma_{ex} P_{in}/(\hbar\omega_L)\right]^{1/2}$, where γ_{ex} is the external loss rate, and $P_{in} = 0.1nW$ is the input driving power. We show that photon antibunching can emerge in a wide range of driving powers, extending from the nanowatt to microwatt regimes (see Fig. S3 in Supplementary information). The other parameters in our work are: $\omega_a/2\pi = \omega_c/2\pi = 460$THz, $\omega_b/2\pi = 30$THz, $Q_a = 10^6$, $Q_c = 46$, $\gamma/2\pi = 30$GHz, $J/2\pi = 3$THz. For the Fabry-Pérot cavities, the cavity quality factor $Q \sim 10^5 - 10^7$ [1,69].

The final term in $\widehat{H}_d$ represents the coupling between the cavity field and the parametric amplifier with the parametric gain amplitude Ω and phase θ, which depends on the pump power and phase of the driving parametric amplifier, respectively. To clearly see the interaction relation in this hybrid molecular optomechanical system, we further show the schematic diagram of the equivalent mode-coupling mode in Fig. 1b.

By transforming the system into a rotating frame at the driving frequency ω_L and assuming the condition $\omega_p = 2\omega_L$, the Hamiltonian of the system reads

$$\widehat{H}_2 = \Delta_a \widehat{a}^\dagger \widehat{a} + \Delta_c \widehat{c}^\dagger \widehat{c} + \omega_m \widehat{b}^\dagger \widehat{b} + \widehat{H}_j + \xi(\widehat{c}^\dagger + \widehat{c}) + \Omega(e^{-i\theta}\widehat{a}^{\dagger 2} + e^{i\theta}\widehat{a}^2), \tag{2}$$

where $\Delta_a = \omega_a - \omega_l$, $\Delta_c = \omega_c - \omega_l$. The quantum properties of light can be characterized by the second-order quantum correlation[70]:

$$g^{(2)}(\tau) = \lim_{t\to\infty} \frac{\langle \widehat{a}_1^\dagger(t)\widehat{a}_1^\dagger(t+\tau)\widehat{a}_1(t+\tau)\widehat{a}_1(t)\rangle}{\langle \widehat{a}_1^\dagger(t)\widehat{a}_1(t)\rangle^2}, \tag{3}$$

which is usually measured by Hanbury Brown-Twiss interferometers[71–75]. The condition $g^{(2)}(0) \ll 1$ indicates single-photon blockade with sub-Poissonian photon-number statistics[71,76–78]. By introducing the density matrix of the cavity field $\rho(t)$ and Lindblad superoperator $D[O](\rho) = [O, \rho] = 2O\rho O^\dagger - OO^\dagger\rho - \rho O^\dagger O$, (where $O = a, b, c$), this $g^{(2)}(\tau)$ [or $g^{(2)}(0)$] can be calculated by numerically solving the Lindblad master equation of this system[79,80]:

$$\begin{aligned} L \quad = \quad & -i[H_2,\rho] + \tfrac{\kappa_a(n_a+1)}{2}D[\widehat{a}] + \tfrac{\kappa_a n_a}{2}D[\widehat{a}^\dagger] \\ & + \tfrac{\kappa_c(n_c+1)}{2}D[\widehat{c}] + \tfrac{\kappa_c n_c}{2}D[\widehat{c}^\dagger] \\ & + \tfrac{\gamma(n_b+1)}{2}D[b] + \tfrac{\gamma n_b}{2}D[b^\dagger], \end{aligned} \tag{4}$$

where $n_{b(a,c)} = \left[\exp(\hbar\omega_{b(a,c)}/(k_b T)) - 1\right]^{-1}$ is the mean thermal phonon (photon) number of the mechanical (optical) mode at temperature T, with the Boltzmann constant k_b. The decay rate of the cavity (plasmonic) mode is given by $\kappa_a = \omega_a/Q_a$ ($\kappa_c = \omega_c/Q_c$).

Optimal conditions

To diagonalize the Hamiltonian, we introduce the following unitary operator $\widehat{U}(\beta_0) = e^{\beta_0 \widehat{c}^\dagger \widehat{c}(\widehat{b}^\dagger - \widehat{b})}$, where $\beta_0 = -g_0/\omega_m$. Using the fact that $g_0 \ll \omega_m$, we can safely neglect small exponential terms, allowing the mechanical mode of molecular vibrations to decouple from the plasmonic nanocavity mode. It is easy to make a unitary transformation on the Hamiltonian of the Molecular cavity optomechanical system:

$$\begin{aligned} \widehat{H}_3 = \widehat{U}\widehat{H}_2\widehat{U}^\dagger \quad = \quad & \Delta\widehat{a}^\dagger\widehat{a} + \Delta\widehat{c}^\dagger\widehat{c} + J\left(\widehat{a}^\dagger\widehat{c} + \widehat{a}\widehat{c}^\dagger\right) - G\left(\widehat{c}^\dagger\widehat{c}\right)^2 \\ & + \xi\left(\widehat{c}^\dagger + \widehat{c}\right) + \Omega(\widehat{a}^{\dagger 2}e^{-i\theta} + \widehat{a}^2 e^{i\theta}), \end{aligned} \tag{5}$$

must be increased where $G = \frac{g_0^2}{\omega_m}$. Here, we wrote in a frame where the pump and signal modes' phase space rotates at frequency ω_L. In accordance with the quantum trajectory method[81], the decay of optical can be included in the effective Hamiltonian.

$$\widehat{H}_{eff} = \widehat{H}_3 - \frac{i\kappa_a}{2}\widehat{a}^\dagger\widehat{a} - \frac{i\kappa_c}{2}\widehat{c}^\dagger\widehat{c}. \tag{6}$$

Under the weak-driving condition($\xi \ll \gamma$), the Hilbert space can be restricted to $N = M + N = 3$. The state of this system can be expressed as

$$\left|\psi(t)\right\rangle = \sum_{N=0}^{3}\sum_{m=0}^{N} C_{m,N-m}|m, N-m\rangle, \tag{7}$$

with probability amplitudes $C_{m,N-m}$, which can be obtained by solving the Schrödinger equation

$$i\left|\dot{\psi}(t)\right\rangle = \widehat{H}_{eff}\left|\psi(t)\right\rangle. \tag{8}$$

Based on the effective Hamiltonian $\widehat{H}_{eff}$ and the wave function, we can obtain the steady-state equations of the probability amplitudes. For $C_{00}(t)$, we have $iC_{00}(t) = 0$, while the other amplitudes fulfill the following equations:

$$\begin{aligned} & 0 = \Delta_1 C_{1,0} + JC_{0,1} + \xi C_{1,1}, \\ & 0 = \Delta_2 C_{0,1} + JC_{1,0} + \xi C_{0,0} + \sqrt{2}\xi C_{0,2}, \\ & 0 = 2\Delta_1 C_{2,0} + \sqrt{2}JC_{1,1} + \sqrt{2}\Omega e^{i\theta}C_{0,0}, \\ & 0 = (\Delta_1 + \Delta_2)C_{1,1} + \sqrt{2}JC_{0,2} + \sqrt{2}JC_{2,0} + \xi C_{1,0}, \\ & 0 = 2\Delta_2 C_{0,2} + \sqrt{2}JC_{1,1} + \sqrt{2}\xi C_{0,1}. \end{aligned} \tag{9}$$

Here, we have $\Delta_1 = \Delta_c - \frac{i\kappa_a}{2}$, $\Delta_2 = \Delta_c - G - \frac{i\kappa_c}{2}$.

We obtain the following solutions by considering the initial condition $C_{00}(0) = 1$:

$$\begin{aligned} C_{10} &= \tfrac{J\xi}{\eta_1}, \\ C_{20} &= \tfrac{\sqrt{2}\xi^2 J^2(\Delta_1 + \Delta_2 - G) - \sqrt{2}\Omega e^{i\theta}\eta_1\eta_2}{\eta_1\eta_3}, \end{aligned} \tag{10}$$

where $\eta_1 = \Delta_1\Delta_2 - J^2$, $\eta_2 = \eta_1 + \Delta_2^2 - (\Delta_1 + \Delta_2)G$, $\eta_3 = 2\Delta_1\eta_2 - 2J^2(\Delta_2 - G)$. Since $\left|C_{10}\right|^2 \gg \left|C_{20}\right|^2$ and $\left|C_{10}\right|^2 \gg \left|C_{11}\right|^2$, the second-order correlation function can be written as

$$g^{(2)}(0) = \frac{2\left|C_{20}\right|^2}{\left(\left|C_{10}\right|^2 + 2\left|C_{20}\right|^2 + \left|C_{11}\right|^2\right)^2} \approx \frac{2\left|C_{20}\right|^2}{\left|C_{10}\right|^4}. \tag{11}$$

The photon blockade can occur with $P_{20} = 0$[56,57,59], which can be attributed to the destructive interference among three transition paths, as illustrated in Fig. 2a: $|0,0\rangle \xrightarrow{\Omega} |2,0\rangle$, $|0,0\rangle \xrightarrow{\omega_L} |0,1\rangle \xrightarrow{\omega_L} |0,2\rangle \xrightarrow{\sqrt{2}J} |1,1\rangle \xrightarrow{\sqrt{2}J} |2,0\rangle$, and $|1,0\rangle \xrightarrow{J} |0,1\rangle \xrightarrow{\omega_L} |1,1\rangle \xrightarrow{\sqrt{2}J} |2,0\rangle$. Thus, the optimal parametric gain satisfies

$$\begin{aligned} \Omega_{opt} &= \frac{\left|\xi^2 J^2(\Delta_1 + \Delta_2 - G)\right|}{|\eta_1\,\eta_2|}, \\ \theta_{opt} &= \arg\left[\xi^2 J^2\left(\Delta_1 + \Delta_2 - G\right)\right] - \arg\left(\eta_1\,\eta_2\right). \end{aligned} \tag{12}$$

We plot the second-order correlation function $g^{(2)}(0)$ as a function of detuning and parametric gain amplitude (or phase), as shown in Fig. 2b, c, where the curves represent $g^{(2)}(0) = 0.1$. The robust photon blockade can be achieved across a wide range of detunings by appropriately tuning the parametric gain amplitude and phase. As the detuning $\Delta/2\pi$ decreases, the gain amplitude Ω must be increased to maintain the optimal blockade conditions. We analytically calculated the optimal parametric gain and phase for $\Delta/2\pi = \{-4, -2, 0, 2, 4\}$ THz based on Eq. (12). These analytically

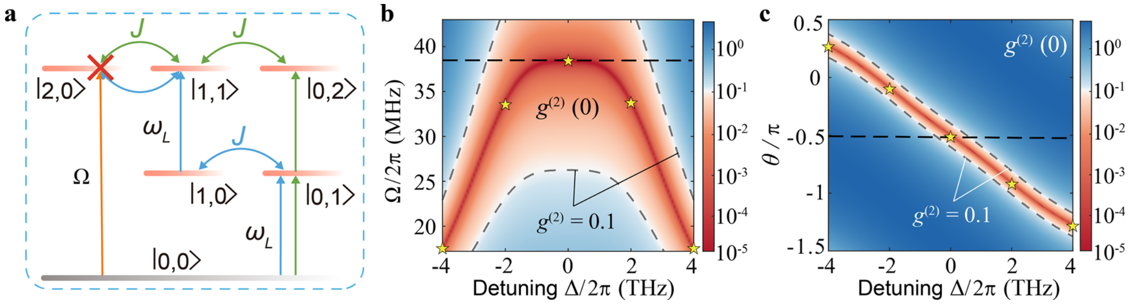

Fig. 2 | The mechanism and optimal parametric gain conditions of molecular optomechanical photon blockade. a The destructive interference of the three transitions from state $|0, 0\rangle$ to state $|2, 0\rangle$ (red, blue, green arrows) prevents two-photon occupation, enabling the unconventional photon blockade effect. **b** Second-order correlation $g^{(2)}(0)$ as a function versus detuning Δ and parametric gain amplitude Ω. **c** Quantum correlation $g^{(2)}(0)$ as a function versus of detuning Δ and parametric gain phase θ. The markers correspond to the analytically obtained optimal points of parametric gain and phase. Here, $P_{\text{in}} = 0.1$ nW, $T = 0$K. The other parameters are given in the main text.

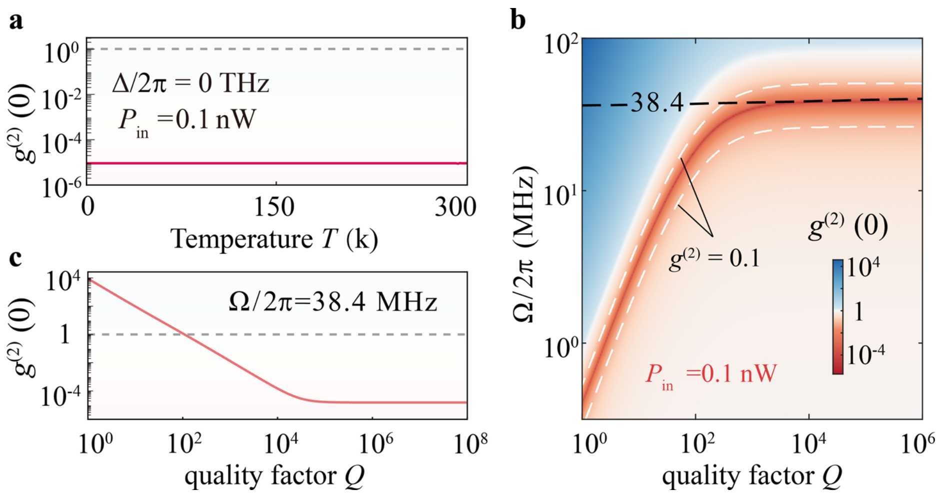

Fig. 3 | Robustness of the molecular optomechanical photon blockade against varying temperature and cavity quality factor. a The second-order correlation function $g^{(2)}(0)$ versus T at driving power $P_{\text{in}} = 0.1$ nW and $\Delta/2\pi = 0$ THz, showing that $g^{(2)}(0) \ll 1$ under room-temperature conditions, thereby demonstrating robust photon blockade in the presence of thermal effects. **b** Influence of the cavity quality factor Q on unconventional photon blockade at an input power of $P_{\text{in}} = 0.1$ nW. Across a broad range of Q values, near-perfect photon blockade can be achieved by properly tuning the Ω, and the optimal Ω is consistent in the high-Q regime. **c** For $\Omega/2\pi = 38.4$ MHz, $g^{(2)}(0)$ remains effectively insensitive to Q for $Q > 10^4$, demonstrating the minimal impact of the cavity quality factor on unconventional photon blockade under these conditions. The other parameters are the same as those in Fig. 2.

obtained optimal points are now marked in Fig. 2b, c, which are in good agreement with the numerical minima of $g^{(2)}(0)$.

Robust photon blockade against temperature and optical dissipation

Our results show that photon blockade in this system exhibits remarkable robustness to temperature variations. As temperature increases, the thermal occupations of phonons ($n_b = [\exp(\hbar\omega_b/(k_b T)) - 1)]^{-1}$) rise, typically weakening photon blockade in conventional optomechanical systems. In contrast, the molecular optomechanical system features an acoustic mode frequency of molecular vibrations that is sufficiently high ($\omega_b/2\pi$ = 30THz) to keep phonon occupation comparatively low ($n_b \approx 0.8$), even at room temperature. While the photon thermal occupation remains negligible, allowing the photon blockade effect to persist essentially undisturbed, as illustrated in Fig. 3a. This behavior is in stark contrast to conventional optomechanical systems, where thermal noise rapidly destroys photon antibunching (see Fig. S1a in the Supplementary Material).

We further find that single-photon blockade is robust against the quality factor of the coupled Fabry-Pérot cavity. As illustrated in Fig. 3b, strong antibunching ($g_2 \ll 1$) is observed at $Q = 1$ by tuning the parametric strength, indicating that single-photon blockade can be achieved even in low-Q cavities. For high-Q cavities, the optimal parametric strength for single-photon blockade stabilizes and does not vary significantly. Hence, as shown in Fig. 3c, once the Fabry-Pérot cavity quality factor Q exceeds 10^4, the parametric gain for unconventional photon blockade remains nearly unchanged, in contrast to conventional optomechanical systems where antibunching strongly depends on cavity dissipation (see Fig. S1b, c in the Supplementary Material).

Oscillation-free photon blockade

Finally, we find that our approach can release the strict requirement of high temporal resolution in photon correlation measurements. As the detuning Δ decreases, the optimal parametric gain amplitude Ω required to achieve photon blockade increases accordingly, while the time-dependent second-order correlation function $g^{(2)}(\tau) = \langle a^\dagger(0)\, a^\dagger(\tau)\, a(\tau)\, a(0)\rangle / \langle a^\dagger a\rangle^2$ gradually becomes oscillation-free. Specifically, for $\Delta/2\pi = -10$THz and -5THz, robust photon blockade is obtained at $\Omega/2\pi$ = 2.1MHz and 11.5MHz, respectively (Fig. 4a, b). In these cases, although $g^{(2)}(0)$ is significantly suppressed, pronounced oscillations still appear in $g^{(2)}(\tau)$ during the temporal evolution (Fig. 4d, e). An excellent agreement between our analytical results and numerical results is shown in Fig. 4. Note that the effect of quantum jumps is ignored (considered) in the semiclassical analytical (quantum master equation) approach[82].

Remarkably, at zero detuning ($\Delta/2\pi$ = 0THz), the minimum value of $g^{(2)}(0)$ is achieved at $\Omega/2\pi$ = 38.4MHz (Fig. 4c). In this regime, the system simultaneously exhibits features of both conventional and unconventional photon blockade: $g^{(2)}(0)$ remains well below unity, while the temporal oscillations in $g^{(2)}(\tau)$ are completely eliminated (Fig. 4f). We show that the temporal oscillations in $g^{(2)}(\tau)$ originate from coherent energy exchange between the two coupled optical modes[56–59]. The underlying physics of oscillation-free photon blockade is the competition between the coherent inter-cavity coupling and the dissipation. (see Fig. S2 in the Supplementary Material). As a result, photon antibunching persists over a prolonged time window of nearly $10\kappa_c$, enabling

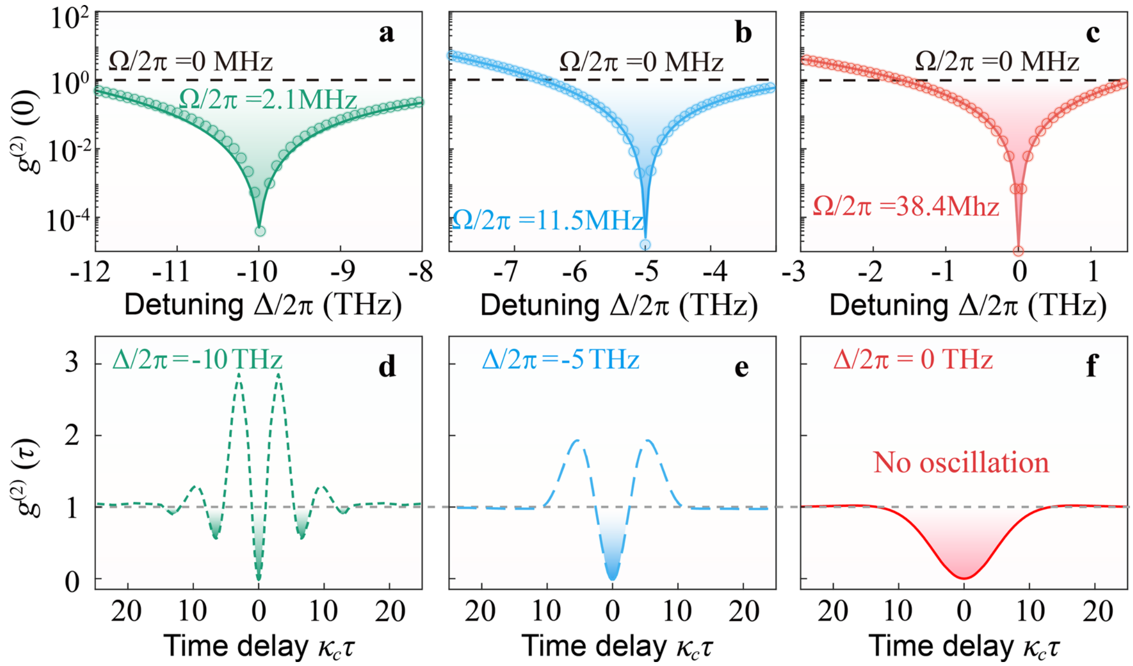

Fig. 4 | Robust and oscillation-free photon blockade over time. For (**a**) $\Delta/2\pi = -10$ THz, **b** $\Delta/2\pi = -5$ THz and **c** $\Delta/2\pi = 0$ THz, the optimal parametric gain amplitude for realizing robust photon blockade is $\Omega/2\pi = 2.1$ MHz, $\Omega/2\pi = 11.5$ MHz and $\Omega/2\pi = 38.4$ MHz, respectively. The curves and markers correspond to the numerical and analytical results, respectively. **d**, **e**, **f** The evolution of the second-order correlation function $g^{(2)}(\tau)$ with respect to the time delay τ/γ, showing no oscillations at $\Delta = 0$, thereby indicating that high temporal resolution is not needed to observe photon blockade in this regime. Here, $P_{\rm in} = 0.1$ nW, and the other parameters are the same as those in Fig. 2.

reliable observation of photon blockade without requiring ultrahigh temporal resolution in correlation measurements.

Discussion

We have proposed how to realize a robust photon blockade scheme based on a hybrid molecular cavity optomechanical system, introducing a degenerate optical parametric amplifier. By tuning the parametric gain amplitude and phase, strong photon antibunching is achieved across a wide range of detuning. Owing to the high-frequency molecular vibrations and enhanced optomechanical coupling, the system exhibits remarkable resilience against variations in temperature and optical dissipation, maintaining nonclassical photon statistics even under room-temperature conditions. Furthermore, the system exhibits both conventional and unconventional photon blockade characteristics, i.e., $g^{(2)}(0)$ remains well below unity while the temporal oscillations in $g^{(2)}(\tau)$ are completely eliminated. This allows photon blockade to be observed without the need for high temporal resolution, improving experimental feasibility.

This work highlights the unique advantages of hybrid molecular cavity optomechanical systems, which combine nanoscale mechanical degrees of freedom with high optical quality factors and strong light-matter interactions. These features make such systems promising platforms for realizing a range of quantum effects beyond photon blockade, including light-motion entanglement[83–86], optomechanical cat states[87–89], photon bundles[90–93], and thermally robust squeezed or correlated states[39,40]. Moreover, the intrinsic resilience of the system to environmental decoherence makes it particularly attractive for applications in quantum sensing and precision measurement under ambient conditions. Our findings offer a foundation for exploring broader functionalities of hybrid optomechanical architectures in integrated quantum photonics.

Methods

Method for constructing the NPoM structure

In molecular optomechanical experiments, the vibrational mode typically originates from self-assembled molecular monolayers, such as thiol-based Raman-active molecules, confined within a NPoM nanogap[27]. The NPoM structure can be practically constructed by bottom-up deposition of metallic nanoparticles onto a mirror coated with a metallic film and separated by an ultrathin molecular spacer, which enables strong plasmon confinement and enhanced optomechanical coupling.

Measurement of the photon blockade in hybrid molecular optomechanical systems

To assess the robust photon blockade in the hybrid molecular optomechanical systems, we outline a feasible measurement scheme for the output-field intensity and the second-order correlation function $g^{(2)}(\tau)$ of the physical cavity mode. In principle, a weak probe field generated by a tunable narrow-linewidth laser can be injected into the nanocavity. The polarization and driving strength can be controlled using standard polarization controllers and variable optical attenuators, while the transmitted signal from the optical cavity output port can be monitored by photodetectors[94].

The photon blockade can be characterized by measuring the normalized second-order correlation function $g^{(2)}(\tau)$ of the output field using Hanbury Brown-Twiss interferometers[71–75]. The output field is split into two paths and detected by single-photon avalanche photodiodes, and the coincidence counts are recorded as a function of the delay time τ. From the record counts, the $g^{(2)}(\tau)$ can be inferred by using the procedures discussed in refs. 71,94. Unlike many OPA-assisted proposals that involve Bogoliubov modes or squeezed-field detection, the present scheme relies on the correlation function of the cavity-field operator. Moreover, the absence of temporal oscillations in $g^{(2)}(\tau)$ releases the strict condition of high temporal resolution in experimental detection.

Data availability

All relevant data that support the figures within this paper and other findings of this study are available from the corresponding authors upon reasonable request.

Code availability

All relevant code supports the figures within this paper, and other findings of this study are available from the corresponding authors upon reasonable request.

Received: 28 August 2025; Accepted: 5 March 2026;
Published online: 23 March 2026

References

1. Aspelmeyer, M., Kippenberg, T. J. & Marquardt, F. Cavity optomechanics. *Rev. Mod. Phys.* **86**, 1391 (2014).
2. Metcalfe, M. Applications of cavity optomechanics. *Appl. Phys. Rev.* **1**, 031105 (2014).
3. Aspelmeyer, M., Meystre, P. & Schwab, K. Quantum optomechanics. *Phys. Today* **65**, 29 (2012).
4. Kippenberg, T. J. & Vahala, K. J. Cavity optomechanics: back-action at the mesoscale. *Science* **321**, 1172 (2008).
5. Brennecke, F., Ritter, S., Donner, T. & Esslinger, T. Cavity optomechanics with a Bose-Einstein condensate. *Science* **322**, 235 (2008).
6. Pirkkalainen, J.-M. et al. Cavity optomechanics mediated by a quantum two-level system. *Nat. Commun.* **6**, 6981 (2015).
7. Li, B.-B., Ou, L., Lei, Y. & Liu, Y.-C. Cavity optomechanical sensing. *Nanophotonics* **10**, 2799 (2021).
8. Zhu, G.-L., Hu, C.-S., Wu, Y. & Lu, X.-Y. Cavity optomechanical chaos. *Fundam. Res.* **3**, 63 (2023).
9. Xu, J. et al. Single-cavity loss-enabled nanometrology. *Nat. Nanotechnol.* **19**, 1472–1477 (2024).
10. Benz, F. et al. Single-molecule optomechanics in “picocavities”. *Science* **354**, 726 (2016).
11. Roelli, P., Galland, C., Piro, N. & Kippenberg, T. J. Molecular cavity optomechanics as a theory of plasmon-enhanced Raman scattering. *Nat. Nanotechnol.* **11**, 164 (2016).
12. Esteban, R., Baumberg, J. J. & Aizpurua, J. Molecular optomechanics approach to surface-enhanced Raman scattering. *Acc. Chem. Res.* **55**, 1889–1899 (2022).
13. Ashrafi, S. M., Malekfar, R., Bahrampour, A. R. & Feist, J. Optomechanical heat transfer between molecules in a nanoplasmonic cavity. *Phys. Rev. A* **100**, 013826 (2019).
14. Yin, B. et al. Molecular optomechanically induced transparency. *Phys. Rev. A* **111**, 043507 (2025).
15. Chen, W. et al. Continuous-wave frequency upconversion with a molecular optomechanical nanocavity. *Science* **374**, 1264 (2021).
16. Xomalis, A. et al. Detecting mid-infrared light by molecular frequency upconversion in dual-wavelength nanoantennas. *Science* **374**, 1268 (2021).
17. Zou, F., Du, L., Li, Y. & Dong, H. Amplifying frequency up-converted infrared signals with a molecular optomechanical cavity. *Phys. Rev. Lett.* **132**, 153602 (2024).
18. Liu, J. & Zhu, K.-D. Room temperature optical mass sensor with an artificial molecular structure based on surface plasmon optomechanics. *Photon. Res.* **6**, 867 (2018).
19. Liu, J. & Zhu, K.-D. Coupled quantum molecular cavity optomechanics with surface plasmon enhancement. *Photon. Res.* **5**, 450 (2018).
20. Tabatabaei, M. et al. Tunable 3D plasmonic cavity nanosensors for surface-enhanced Raman spectroscopy with sub-femtomolar limit of detection. *ACS Photon.* **2**, 752 (2015).
21. Zhang, Y., Aizpurua, J. & Esteban, R. Optomechanical collective effects in surface-enhanced Raman scattering from many molecules. *ACS Photon.* **7**, 1676 (2020).
22. Jakob, L. A. et al. Giant optomechanical spring effect in plasmonic nano- and picocavities probed by surface-enhanced Raman scattering. *Nat. Commun.* **14**, 3291 (2023).
23. Sadhanasatish, T. et al. A molecular optomechanics approach reveals functional relevance of force transduction across talin and desmoplakin. *Sci. Adv.* **9**, eadg3347 (2023).
24. Zhu, B., Meystre, P., Zhang, W. & Zhang, K. Autonomous quantum heat engine enabled by molecular optomechanics and hysteresis switching. *Phys. Rev. A* **112**, 043508 (2025).
25. Huang, J., Lei, D., Agarwal, G. S. & Zhang, Z. Collective quantum entanglement in molecular cavity optomechanics. *Phys. Rev. B* **110**, 184306 (2024).
26. Zhang, T., Wang, Y. & Hua, Q. Plasmonic-photonic crystal hybrid devices for optical characterization. *J. Phys. D Appl. Phys.* **57**, 363001 (2024).
27. Shlesinger, I., Vandersmissen, J., Oksenberg, E., Verhagen, E. & Koenderink, A. F. Hybrid cavity-antenna architecture for strong and tunable sideband-selective molecular Raman scattering enhancement. *Sci. Adv.* **9**, eadj4637 (2023).
28. Yu, H.-Y. et al. Strong molecule-light entanglement with molecular cavity optomechanics. *Phys. Rev. Lett.* **136**, 013602 (2026).
29. Shlesinger, I., Cognée, K. G., Verhagen, E. & Koenderink, A. F. Integrated molecular optomechanics with hybrid dielectric-metallic resonators. *ACS Photon.* **8**, 3506–3516 (2021).
30. Dezfouli, M. K., Gordon, R. & Hughes, S. Molecular optomechanics in the anharmonic cavity-qed regime using hybrid metal-dielectric cavity modes. *ACS Photon.* **6**, 1400–1408 (2019).
31. Barreda, A. I. et al. Hybrid photonic-plasmonic cavities based on the nanoparticle-on-a-mirror configuration. *Photon. Res.* **9**, 2398–2419 (2021).
32. Zhang, Y. et al. Miniature computational spectrometer with a plasmonic nanoparticles-in-cavity microfilter array. *Nat. commun.* **15**, 3807 (2024).
33. Shen, Y. R. *Principles of Nonlinear Optics* (Wiley-Interscience, NY, USA, 1984).
34. U'Ren, A. B. et al. Generation of pure-state single-photon wavepackets by conditional preparation based on spontaneous parametric downconversion. *Laser Phys. Lett.* **15**, 146–160 (2005).
35. Mosley, P. J. et al. Heralded generation of ultrafast single photons in pure quantum states. *Phys. Rev. Lett.* **100**, 133601 (2008).
36. Harris, S. E. Chirp and compress: toward single-cycle biphotons. *Phys. Rev. Lett.* **98**, 063602 (2007).
37. Crouch, D. D. Broadband squeezing via degenerate parametric amplification. *Phys. Rev. A* **38**, 508–511 (1988).
38. Kashiwazaki, T. et al. Continuous-wave 6-db-squeezed light with 2.5-thz-bandwidth from single-mode ppln waveguide. *APL Photon.* **5**, 036104 (2020).
39. Qin, W., Miranowicz, A. & Nori, F. Beating the 3 db limit for intracavity squeezing and its application to nondemolition qubit readout. *Phys. Rev. Lett.* **129**, 123602 (2022).
40. Kawasaki, A. et al. Broadband generation and tomography of non-Gaussian states for ultra-fast optical quantum processors. *Nat. Commun.* **15**, 9075 (2024).
41. Yan, Z.-H. et al. Generation of non-classical states of light and their application in deterministic quantum teleportation. *Fundam. Res.* **1**, 43–49 (2021).
42. Hou, F.-Y. et al. Experimental generation of optical non-classical states of light with 1.34 μ m wavelength. *Eur. Phys. J. D* **62**, 433–437 (2011).
43. Tang, L. et al. Quantum squeezing induced optical nonreciprocity. *Phys. Rev. Lett.* **128**, 083604 (2022).
44. Lu, T.-X. et al. Quantum squeezing induced nonreciprocal phonon laser. *Sci. China Phys. Mech. Astronom.* **67**, 260312 (2024).
45. Qin, W. et al. Exponentially enhanced light-matter interaction, cooperativities, and steady-state entanglement using parametric amplification. *Phys. Rev. Lett.* **120**, 093601 (2018).
46. Qin, W., Miranowicz, A., Jing, H. & Nori, F. Generating long-lived macroscopically distinct superposition states in atomic ensembles. *Phys. Rev. Lett.* **127**, 093602 (2021).

47. Chen, Y.-H., Qin, W., Wang, X., Miranowicz, A. & Nori, F. Shortcuts to adiabaticity for the quantum Rabi model: efficient generation of giant entangled cat states via parametric amplification. *Phys. Rev. Lett.* **126**, 023602 (2021).
48. Jiao, Y.-F. et al. Tripartite quantum entanglement with squeezed optomechanics. *Laser Photon. Rev.* **18**, 2301154 (2024).
49. Wang, J., Zhang, Q. & Jing, H. Quantum weak torque sensing with squeezed optomechanics. *Phys. Rev. A* **110**, 033505 (2024).
50. Zhang, S.-D. et al. Squeezing-enhanced quantum sensing with quadratic optomechanics. *Opt. Quantum* **2**, 222–229 (2024).
51. Lü, X.-Y. et al. Squeezed optomechanics with phase-matched amplification and dissipation. *Phys. Rev. Lett.* **114**, 093602 (2015).
52. Wang, D.-Y. et al. Squeezing-induced nonreciprocal photon blockade in an optomechanical microresonator. *Opt. Express* **31**, 22343–22357 (2023).
53. Shen, C.-P. et al. Tunable nonreciprocal photon correlations induced by directional quantum squeezing. *Phys. Rev. A* **108**, 023716 (2023).
54. Vaneph, C. et al. Observation of the unconventional photon blockade in the microwave domain. *Phys. Rev. Lett.* **121**, 043602 (2018).
55. Snijders, H. J. et al. Observation of the unconventional photon blockade. *Phys. Rev. Lett.* **121**, 043601 (2018).
56. Liew, T. C. H. & Savona, V. Single photons from coupled quantum modes. *Phys. Rev. Lett.* **104**, 183601 (2010).
57. Bamba, M., Imamoğlu, A., Carusotto, I. & Ciuti, C. Origin of strong photon antibunching in weakly nonlinear photonic molecules. *Phys. Rev. A* **83**, 021802 (2011).
58. Xu, X. W. & Li, Y. Strong photon antibunching of symmetric and antisymmetric modes in weakly nonlinear photonic molecules. *Phys. Rev. A* **90**, 033809 (2014).
59. Flayac, H. & Savona, V. Unconventional photon blockade. *Phys. Rev. A* **96**, 053810 (2017).
60. Li, B., Huang, R., Xu, X., Miranowicz, A. & Jing, H. Nonreciprocal unconventional photon blockade in a spinning optomechanical system. *Photonics Res.* **7**, 630 (2019).
61. Jabri, H. & Eleuch, H. Enhanced unconventional photon-blockade effect in one- and two-qubit cavities interacting with nonclassical light. *Phys. Rev. A* **106**, 023704 (2022).
62. Shen, H. Z., Wang, Q., Wang, J. & Yi, X. X. Nonreciprocal unconventional photon blockade in a driven dissipative cavity with parametric amplification. *Phys. Rev. A* **101**, 013826 (2020).
63. Gou, C. & Hu, X. Simultaneous nonreciprocal photon blockade in two coupled spinning resonators via Sagnac-Fizeau shift and parametric amplification. *Phys. Rev. A* **108**, 043723 (2023).
64. Wang, D.-Y. et al. Enhanced photon blockade in an optomechanical system with parametric amplification. *Opt. Lett.* **45**, 2604–2607 (2020).
65. Xie, H., He, L.-W., Shang, X. & Lin, X.-M. Photon blockade in cavity optomechanics via parametric amplification. *Adv. Quantum Technol.* **7**, 2400065 (2024).
66. Peng, W. et al. Construction of nanoparticle-on-mirror nanocavities and their applications in plasmon-enhanced spectroscopy. *Chem. Sci.* **15**, 2697–2711 (2024).
67. Hu, H. et al. Nanoparticle-on-mirror pairs: building blocks for remote spectroscopies. *Nanophotonics* **11**, 5153–5163 (2022).
68. Li, Y. et al. Boosting light matter interactions in plasmonic nanogaps. *Adv. Mater.* **36**, 2405186 (2024).
69. Galinskiy, I., Tsaturyan, Y., Parniak, M. & Polzik, E. S. Phonon counting thermometry of an ultracoherent membrane resonator near its motional ground state. *Optica* **7**, 718–725 (2020).
70. Glauber, R. J. The quantum theory of optical coherence. *Phys. Rev.* **130**, 2529 (1963).
71. Birnbaum, K. M. et al. Photon blockade in an optical cavity with one trapped atom. *Nature (London)* **436**, 87 (2005).
72. Dayan, B. et al. A photon turnstile dynamically regulated by one atom. *Science* **319**, 1062 (2008).
73. Hamsen, C., Tolazzi, K. N., Wilk, T. & Rempe, G. Strong coupling between photons of two light fields mediated by one atom. *Nat. Phys.* **14**, 885 (2018).
74. Hennessy, K. et al. Quantum nature of a strongly coupled single quantum dot–cavity system. *Nature (London)* **445**, 896 (2007).
75. Faraon, A. et al. Coherent generation of non-classical light on a chip via photon-induced tunnelling and blockade. *Nat. Phys.* **4**, 859 (2008).
76. Imamog̅lu, A., Schmidt, H., Woods, G. & Deutsch, M. Strongly Interacting Photons in a Nonlinear Cavity. *Phys. Rev. Lett.* **79**, 1467 (1997).
77. Scully, M. O. & Zubairy, M. S. *Quantum Optics* (Cambridge University Press, Cambridge, England, 1997).
78. Agarwal, G. S. *Quantum Optics* (Cambridge University Press, Cambridge, England, 2012).
79. Johansson, J., Nation, P. & Nori, F. QuTiP: an open-source Python framework for the dynamics of open quantum systems. *Comput. Phys. Commun.* **183**, 1760 (2012).
80. Johansson, J., Nation, P. & Nori, F. QuTiP 2: a Python framework for the dynamics of open quantum systems. *Comput. Phys. Commun.* **184**, 1234 (2013).
81. Plenio, M. B. & Knight, P. L. The quantum-jump approach to dissipative dynamics in quantum optics. *Rev. Mod. Phys.* **70**, 101 (1998).
82. Minganti, F., Miranowicz, A., Chhajlany, R. W. & Nori, F. Quantum exceptional points of non-Hermitian Hamiltonians and Liouvillians: the effects of quantum jumps. *Phys. Rev. A* **100**, 062131 (2019).
83. Wang, Y.-D. & Clerk, A. A. Reservoir-engineered entanglement in optomechanical systems. *Phys. Rev. Lett.* **110**, 253601 (2013).
84. Jiao, Y.-F. et al. Nonreciprocal optomechanical entanglement against backscattering losses. *Phys. Rev. Lett.* **125**, 143605 (2020).
85. Liu, J.-X., Yang, J.-Y., Lu, T.-X., Jiao, Y.-F. & Jing, H. Phase-controlled robust quantum entanglement of remote mechanical oscillators. *Phys. Rev. A* **109**, 023519 (2024).
86. Li, Y. et al. Vector optomechanical entanglement. *Nanophotonics* **11**, 67–77 (2022).
87. Hauer, B. D., Combes, J. & Teufel, J. D. Nonlinear sideband cooling to a cat state of motion. *Phys. Rev. Lett.* **130**, 213604 (2023).
88. Li, B. et al. Optomechanical schrödinger cat states in a cavity Bose-Einstein condensate. *Fundamental Res.* **3**, 15–20 (2023).
89. Liao, J.-Q. & Tian, L. Macroscopic quantum superposition in cavity optomechanics. *Phys. Rev. Lett.* **116**, 163602 (2016).
90. Muńoz, C. S. et al. Emitters of n-photon bundles. *Nat. Photonics* **8**, 550–555 (2014).
91. Bin, Q., Lü, X.-Y., Laussy, F. P., Nori, F. & Wu, Y. *n*-phonon bundle emission via the Stokes process. *Phys. Rev. Lett.* **124**, 053601 (2020).
92. Bin, Q., Wu, Y. & Lü, X.-Y. Parity-symmetry-protected multiphoton bundle emission. *Phys. Rev. Lett.* **127**, 073602 (2021).
93. Zou, F., Li, Y. & Liao, J.-Q. Dynamical n-photon bundle emission. *New J. Phys.* **25**, 043027 (2023).
94. McKeever, J. et al. Deterministic generation of single photons from one atom trapped in a cavity. *Science* **303**, 1992–1994 (2004).

Acknowledgements

The authors thank X.-W. Xu for helpful discussions. H.J. is supported by the National Key R\&D Program (Grant No. 2024YFE0102400), the National Natural Science Foundation of China (Grants No.~12421005), and the Hunan Major Sci-Tech Program (Grant No. 2023ZJ1010). R.H. is supported by the RIKEN Special Postdoctoral Researchers (SPDR) program. X.-W.X. is supported by the Innovation Program for Quantum Science and Technology (Grant No. 2024ZD0301000). T.-X.L. is supported by the NSFC (Grant No. 12565001, 12205054) and the Natural Science Foundation of Jiangxi Province (No. 20252BAC200163). F.N. is supported in part by the Japan Science and Technology Agency (JST)[via the CREST Quantum Frontiers program Grant No. JPMJCR24I2, the Quantum Leap Flagship Program (Q-LEAP), and the Moonshot R\&D Grant No. JPMJMS256E].

Author contributions

H.J. conceived the idea. R.H. and H.J. supervised the project. J.T. performed the research guided by R.H. and H.J. J.T. analyzed the theoretical and numerical results with the help of R.H., B.-J.L., and B.Y. J.T. wrote the manuscript with contributions from R.H., F.N., T.-X.L., and H.J. All authors contributed to the completion of the paper.

Competing interests

The authors declare no competing interests.

Additional information

Supplementary information The online version contains supplementary material available at https://doi.org/10.1038/s41534-026-01220-3.

Correspondence and requests for materials should be addressed to Ran Huang or Hui Jing.

Reprints and permissions information is available at http://www.nature.com/reprints

Publisher's note Springer Nature remains neutral with regard to jurisdictional claims in published maps and institutional affiliations.